

Rational Approximation of Nonlinear Systems Via NL-VF

Abner Ramirez , Senior Member, IEEE, Bjørn Gustavsen , Fellow, IEEE, and Isaias Ramirez, Member, IEEE

Abstract—This paper presents an alternative vector fitting (VF)-based approach to generate a rational model of nonlinear system behaviors. The proposed approach, named here as nonlinear VF (NL-VF), has its fundament in the previously proposed time-domain VF (TD-VF). TD-VF generates rational models using TD input/output responses and numerical convolution. Unlike TD-VF, NL-VF utilizes input/output vectors in the frequency domain (FD) to produce a rational approximation of the corresponding transfer function/matrix. The input/output FD vectors are obtained in this paper by a numerical Laplace transform (NLT) algorithm. Alternatively, input/output TD vectors available from any solution algorithm can be transformed to FD via NLT and used in the NL-VF approach. Computational efficiency and accuracy of the NL-VF are compared with the TD-VF technique for the single-phase case. It is demonstrated that NL-VF gives more accurate results than TD-VF, in particular when the data is calculated from a time-window, which does not capture the system slow dynamics. Also, unlike TD-VF, NL-VF can handle in a natural way FD weighting, thus exhibiting error control. The proposed approach is applied in this paper to 1) a boost converter circuit, and 2) a network involving simultaneously a three-phase grid-tied photovoltaic (PV) system and a nonlinear reactor load.

Index Terms—Curve fitting, frequency domain analysis, frequency domain synthesis, nonlinear systems.

I. INTRODUCTION

RATIONAL approximation of linear systems permits to generate wide-band state space models amenable for transient simulation studies [1], [2]. The main characteristics of such models are: a) they provide a dynamic response close to that of the original system, b) they are easy to implement in a computer algorithm, and c) they result in fast simulations with little memory usage.

VF is a mature and widely applied technique for rational approximation of linear system behaviors. Its main applications are in high-voltage power networks and high-speed electronics, for the modeling of components and sub-systems. Classical

VF, as it has been known since 1999, employs the transfer function data, obtained either from analytical closed-form or by numerical data, in the s -domain (i.e., FD) [2]. A number of variants have since been introduced, e.g., formulations in time domain (TD-VF) [3] and z -domain (ZD-VF) [4]. Also, the computational performance has been improved by introduction of relaxation [5], orthonormal basis functions [6], and usage of an instrumental variable [7]. VF in TD (TD-VF) utilizes TD input/output transient variables and applies the convolution concept to find a solution for the rational approximation problem [8]. An alternative method is the autoregressive moving average (ARMA) model, which uses a set of discrete differential equations from the z -domain data, which in its turn, can be obtained from the FD [8]. A thorough comparison in [8] shows that TD-VF is more accurate than ARMA and ZD-VF.

This paper focuses on rational models of nonlinear networks, assumed here as those involving nonlinear loads and/or time-periodic components, such as PV generators. For such systems, their transfer function may not be amenable for direct rational approximation due to involved nonlinear elements or frequency cross-coupling generated by switching dynamics [9], [10], [11]. Hence, a FD solution method can initially be used for calculating frequency responses, i.e., input $\mathbf{X}(s)$ and output $\mathbf{Y}(s)$ vectors [11]–[12]. Alternatively, their TD counterparts $x(t)$ and $y(t)$ can be obtained from simulation software tools [13], [14], [15]. Afterwards, with input/output variables known, TD-VF, for example, can be used to characterize the nonlinear system behaviors. Currently, there are a few FD-based methods to calculate $\mathbf{X}(s)$ and output $\mathbf{Y}(s)$ of nonlinear networks, noting that most existing FD-based methods focus on linear networks/components [16], [17], [19]. Among those methods, the NLT is adopted in this paper due to its robustness and accuracy [19]. The NLT has been applied, besides linear systems, to nonlinear loads and inverter-based generators [11], [12], generating both $\mathbf{X}(s)$ and $\mathbf{Y}(s)$ in a natural s -domain.

This paper proposes the NL-VF as an alternative approach to nonlinear systems FD characterization. NL-VF has its fundament in the previously published TD-VF, noting that the former utilizes input/output variables in the FD for the transfer function characterization, as opposed to TD-VF, which uses their TD counterparts. It is important to mention that, regardless the solution method utilized to solve the nonlinear system (which may rely on its linearized version); the proposed approach utilizes input/output FD variables. That is, the proposed approach can generate a rational approximation of the nonlinear behavior of the system.

Manuscript received 5 July 2022; revised 7 October 2022; accepted 3 December 2022. Date of publication 6 December 2022; date of current version 23 May 2023. Paper no. TPWRD-01002-2022. (Corresponding author: Abner Ramirez.)

Abner Ramirez is with the Center for Research and Advanced Studies of Mexico (CINVESTAV) Campus Guadalajara, 45019 Guadalajara, Mexico, on sabbatical leave from the Polytechnique of Montreal, Montreal, Canada (e-mail: abner.ramirez@cinvestav.mx).

Bjørn Gustavsen is with the SINTEF Energy Research, N-7465 Trondheim, Norway (e-mail: bjorn.gustavsen@sintef.no).

Isaias Ramirez is with the National Institute of Electrical and Clean Energies (INEEL), 62490 Cuernavaca, Mexico (e-mail: iramirez@ineel.mx).

Color versions of one or more figures in this article are available at <https://doi.org/10.1109/TPWRD.2022.3227132>.

Digital Object Identifier 10.1109/TPWRD.2022.3227132

0885-8977 © 2022 IEEE. Personal use is permitted, but republication/redistribution requires IEEE permission. See <https://www.ieee.org/publications/rights/index.html> for more information.

TD-VF was originally conceived to create models from computationally expensive simulations, e.g., TD finite element simulations. TD-VF has the nice ability to generate a model using a truncated TD response, and the model will be accurate when applied to a simulation length not exceeding the time record from which it was extracted [8]. But for long simulation records (thousands of time steps), TD-VF becomes very slow. Also, there is an issue with controlling the accuracy, i.e., how to deal with weighting in TD-VF. In other words, so far one cannot apply weight to individual frequency components in TD-VF, e.g., inverse magnitude weighting for relative error control. On the other hand, NL-VF can handle frequency domain weighting in a direct way, allowing accuracy control. Another advantage of NL-VF over TD-VF is that the former avoids convolution operation in TD and its corresponding time approximation, which can become a source of inaccuracy.

A major difference between classical VF and the proposed NL-VF can be stated as follows. Classical VF requires the knowledge of a transfer function obtained either analytically or by measurements; such transfer function is approximated by a rational function involving a set of poles/residues. In classical VF there is no need of knowing input/output variables. On the other hand, NL-VF uses input/output variables to provide a rational approximation of an (unknown) transfer function. This feature by NL-VF makes it applicable to systems involving electronic switches and nonlinear components.

Section II presents the basic relations of TD-VF, which is taken as basis for the proposed NL-VF approach. The NL-VF is described in Section III while Sections IV and V describe two case studies. Section VI concludes the paper.

II. TD-VF BASIC RELATIONS

The basic relations of the TD-VF technique are described below. The details of TD-VF can be found in [3].

The main objective is to approximate a given $P \times Q$ transfer matrix $\mathbf{H}(s)$ of a system by rational functions using an N -th order pole-residue model (1). Matrix \mathbf{H}_∞ corresponds to the direct coupling matrix. The model uses a common pole set $\{p_n\}$ for all elements within the associated residue matrices $\{\mathbf{R}_n\}$.

$$\mathbf{H}(s) \approx \sum_{n=1}^N \frac{\mathbf{R}_n}{s - p_n} + \mathbf{H}_\infty. \quad (1)$$

The approximation (fitting) is performed via the following two steps.

A. Poles Calculation

To identify the dominant poles of the system, a scalar weighting function is introduced, as in (2), where $\{q_n\}$ is an initial set of known poles which can be chosen as indicated in [2].

$$\sigma(s) = 1 + \sum_{n=1}^N \frac{k_n}{s - q_n} = \frac{\prod_{n=1}^N (s - z_n)}{\prod_{n=1}^N (s - q_n)}. \quad (2)$$

Considering that both input $\mathbf{X}(s)$ and output $\mathbf{Y}(s)$ are available, the following approximation holds [3]:

$$\left[1 + \sum_{n=1}^N \frac{k_n}{s - q_n} \right] \mathbf{Y}(s) = \left[\sum_{n=1}^N \frac{\mathbf{M}_n}{s - q_n} + \mathbf{M}_\infty \right] \mathbf{X}(s). \quad (3)$$

The set of residues $\{k_n\}$ permits to calculate the zeros of $\sigma(s)$ which correspond to a new set of poles $\{p_n\}$. At this point, the new set $\{p_n\}$ can be used within a pole relocation scheme to obtain a better poles estimate.

To calculate the set $\{k_n\}$, TD-VF formulates problem (3) as a least squares (LS) problem using TD input $x(t)$ and output $y(t)$ as variables. First, $x(t)$ and $y(t)$ are found by applying the inverse Laplace transform to $\mathbf{X}(s)$ and $\mathbf{Y}(s)$, or they can be obtained via simulations or measurements. Then, the concept of TD convolution is applied to (3). Finally, the convolution integrals are numerically discretized by using linear interpolation, which corresponds to applying first-order infinite impulse response (IIR) filters [3]. The reader is referred to [3] for the corresponding TD expressions. Usage of trapezoidal rule is often preferable when applying TD-VF to waveforms obtained by EMT-type simulations software [8]. The terms involving FD products $\mathbf{X}(s)/(s - q)$ or $\mathbf{Y}(s)/(s - q)$ in (3) are then solved by applying the trapezoidal rule to the corresponding differential equation.

B. Residues Calculation

The obtained set of poles $\{p_n\}$ is used to calculate the matrices \mathbf{R}_n and \mathbf{H}_∞ in (1), expressed in terms of $\mathbf{X}(s)$ and $\mathbf{Y}(s)$ as

$$\mathbf{Y}(s) = \left[\sum_{n=1}^N \frac{\mathbf{R}_n}{s - p_n} + \mathbf{H}_\infty \right] \mathbf{X}(s). \quad (4)$$

In the TD-VF approach, (4) is solved in the LS sense similar to (3), i.e., using TD variables and applying both the convolution concept and IIR filters (trapezoidal rule).

III. DESCRIPTION OF NL-VF

The proposed approach applies the two main steps described in Section II in which poles and residues calculation are based on the FD input/output vector variables, $\mathbf{X}(s)$ and $\mathbf{Y}(s)$, without resorting to a TD formulation. These variables can be obtained, for example, from a FD-based solution method; the NLT is adopted in this paper due to its accuracy and robustness [19]. Alternatively, $x(t)$ and $y(t)$ can be obtained from a simulation software and be transformed to FD via NLT, then the fitting is applied to obtain the rational model. The flow diagram of Fig. 1 describes the abovementioned two options; this paper applies the one at the left-hand-side (FD-based) while the other (EMT-type simulation) is left for a subsequent research work.

For simplicity of illustration, a 3-terminal case is described next. The extension to the general multi-input multi-output (MIMO) case is straightforward.

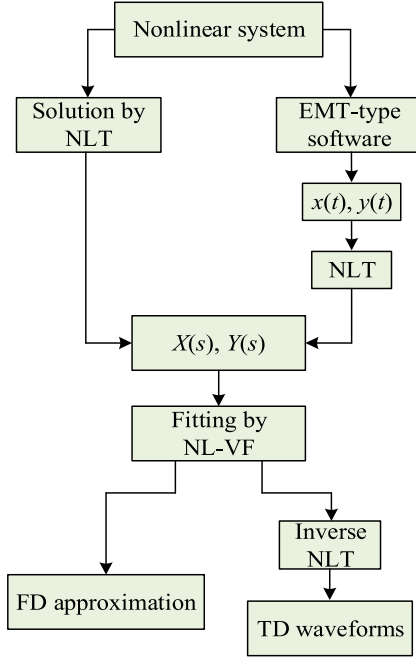


Fig. 1. Input options for the proposed NL-VF approach.

A. Poles Identification

The set of residues $\{k_n\}$, which permits to calculate the new set of poles $\{p_n\}$ as the zeros of $\sigma(s)$, is calculated by solving (3) in the LS sense. Consider a case with n_1 real poles and n_2 complex poles; then (3) can be expressed as

$$\left[1 + \sum_{n=1}^{n_1} \frac{k_n}{s - q_n} + \sum_{n=1}^{n_2} \frac{k'_n}{s - q'_n} \right] \mathbf{Y}(s) = \left[\sum_{n=1}^{n_1} \frac{\mathbf{M}_n}{s - q_n} + \sum_{n=1}^{n_2} \frac{\mathbf{M}'_n}{s - q'_n} + \mathbf{M}_\infty \right] \mathbf{X}(s). \quad (5)$$

Equation (5) is evaluated for M frequencies, resulting in an overdetermined system of the form (details in Appendix B):

$$\mathbf{A}\mathbf{x} = \mathbf{b}. \quad (6)$$

In (6), matrix \mathbf{A} contains either products between $\mathbf{X}(s)$ or $\mathbf{Y}(s)$ and terms of the type $1/(s - q_n)$, or evaluation of $\mathbf{X}(s)$ itself, for $s = s_1, s_2, \dots, s_M$ (see Appendix B). Note that both $\mathbf{X}(s)$ or $\mathbf{Y}(s)$ correspond to FD column vectors of dimensions $3M \times 1$. The right-side \mathbf{b} in (6) is $\mathbf{b} = -\mathbf{Y}(s)$. The unknown vector \mathbf{x} in (6) contains the residues $\{k_n\}$ and the residue elements of both matrices \mathbf{M}_n and \mathbf{M}_∞ . Note that symmetry of residue matrices is considered in this paper; thus, for each residue matrix only 6 elements are calculated. Also, note that in this step only the set $\{k_n\}$ is relevant for the calculation of the zeros of $\sigma(s)$.

B. Residues Calculation

The calculated set of poles $\{p_n\}$ from the step above is used to calculate \mathbf{R}_n and \mathbf{H}_∞ in (1). Separating real and complex poles, (1) gives (7) which is evaluated for M frequencies, resulting in an overdetermined system similar to (6). The problem is solved

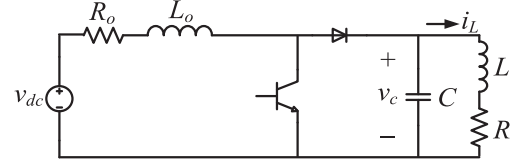


Fig. 2. Boost converter circuit for case study 1.

TABLE I
DATA OF BOOST CONVERTER CIRCUIT

v_{dc}	1,000 V	Source voltage
R_o	0.1 Ohm	Source resistance
L_o	9 mH	Source inductance
f_s	2 kHz	Switching frequency
d	0.5	Duty cycle
R	1 Ohm	Load resistance
L	10 mH	Load inductance
C	2200 μ F	Capacitance

in the LS sense.

$$\mathbf{Y}(s) = \left[\sum_{n=1}^{n_1} \frac{\mathbf{R}_n}{s - p_n} + \sum_{n=1}^{n_2} \frac{\mathbf{R}'_n}{s - p'_n} + \mathbf{H}_\infty \right] \mathbf{X}(s). \quad (7)$$

In this step, matrix \mathbf{A} contains either products between $\mathbf{X}(s)$ and expressions of the type $1/(s - p_n)$, or evaluation of $\mathbf{X}(s)$ itself, for $s = s_1, s_2, \dots, s_M$ (see Appendix B). Also, $\mathbf{b} = \mathbf{Y}(s)$. The unknown vector \mathbf{x} now contains the (upper triangular) residue elements of matrices \mathbf{R}_n and \mathbf{H}_∞ .

In both procedures, poles identification and residues calculation, the corresponding system (6) is formulated such that the poles and residue matrices result real-valued and complex-conjugate, see Appendix B.

IV. CASE STUDY 1: BOOST CONVERTER CIRCUIT

This case study aims at showing the advantages of NL-VF over TD-VF in terms of accuracy, efficiency, and noise immunity. To achieve this, a single-input single-output (SISO) boost converter circuit is utilized.

A. Circuit Description

Consider the boost converter circuit in Fig. 2 with parameters listed in Table I. For this case study, the input and output are assumed to be the DC voltage source and voltage at capacitor terminals, respectively. The solution variables are obtained by an NLT algorithm programmed in Matlab and using a computer with Intel Core i7-8565U CPU@1.8 GHz, 16.0 GB, HD 500 GB. The NLT provides both the FD variable vectors, $V_{dc}(s)$ and $V_c(s)$, fed into the NL-VF algorithm, and the instantaneous values, $v_{dc}(t)$ and $v_c(t)$, utilized in the TD-VF. Note that a well-established relation between time-step length and maximum frequency is obeyed by the NLT [19].

It is mentioned that for inverter-based systems the transfer function involves frequency cross-coupling [9], [10], [11] which

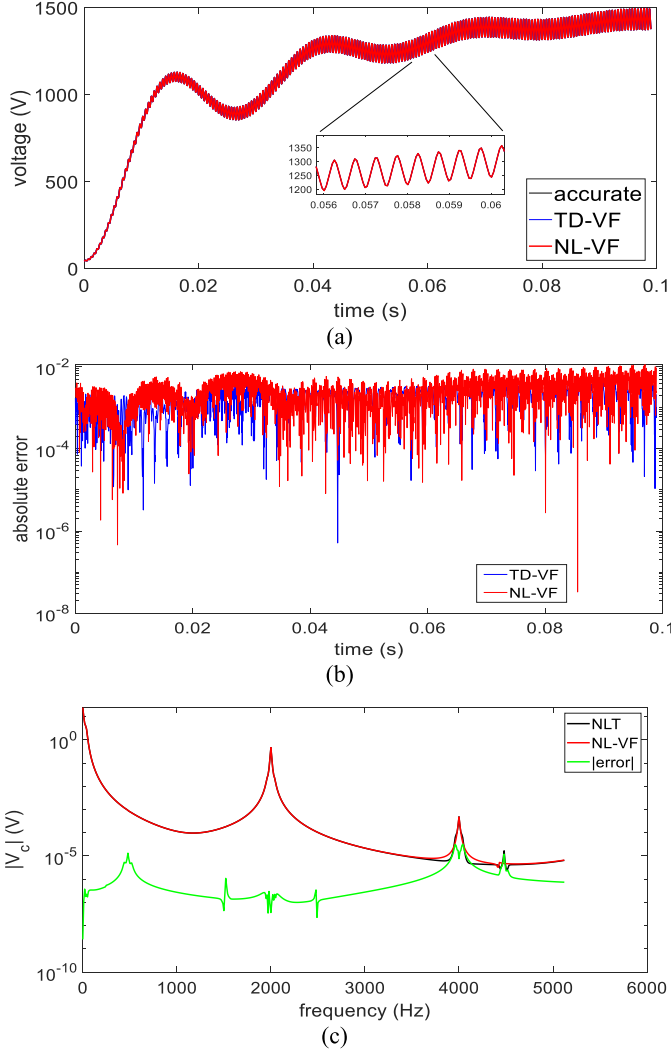


Fig. 3. (a) Capacitor voltage, $v_c(t)$, and its approximations by TD-VF and NL-VF using a time-window of 0.1 s and 2048 samples, (b) absolute errors of approximations, and (c) FD spectrum corresponding to $V_c(s)$.

hinders its direct rational approximation. In other words, instead of having a single-valued element, e.g., $H_{1,1}(s)$, the transfer matrix elements are Toeplitz-type sub-matrices with the frequency content of the switching function. This is confirmed by the FD input/output relation presented in Appendix A for the boost converter circuit of Fig. 2.

B. Numerical Results

Fig. 3(a) presents the “exact” transient waveform $v_c(t)$ (given by the NLT algorithm) and its approximation from the TD-VF and NL-VF fittings, using 2048 samples and a time-window of 0.1 s. With both TD-VF and NL-VF, a model with $N = 40$ poles is calculated using 10 pole relocating iterations. The corresponding absolute errors are shown in Fig. 3(b), indicating a similar accuracy with both modeling approaches. Note that the chosen order of approximation is arbitrary and by increasing it, a smaller error is obtained. The cpu-times by TD-VF and NL-VF are 0.16 s and 0.075 s, respectively. Fig. 3(c) presents the FD spectrum of the output $V_c(s)$, given by NLT, and its

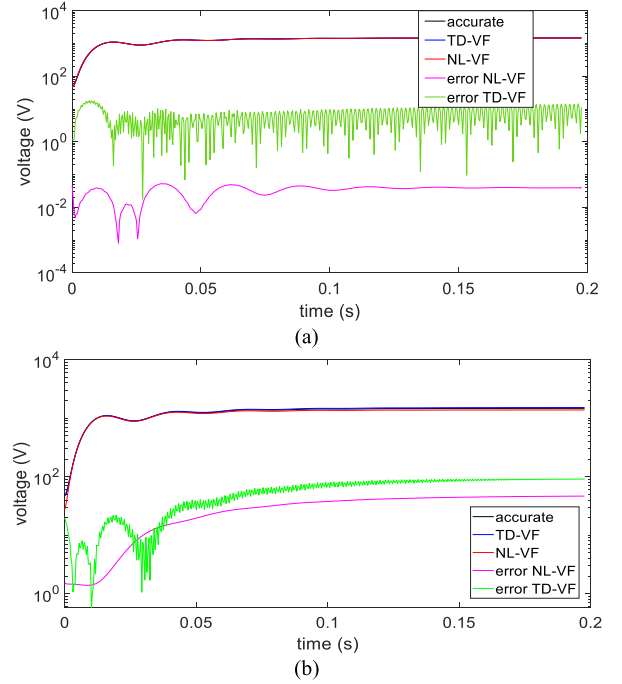


Fig. 4. (a) $v_c(t)$ using a time record of 0.1 s and a simulation time-window of 0.2 s and 512 samples. (b) $v_c(t)$ using a time record of 0.01 s and a simulation time-window of 0.2 s and 512 samples.

approximation given by NL-VF. The peaks in the FD spectrum correspond to the switching frequency of 2 kHz and its first harmonic.

Based on the obtained rational models by TD-VF and NL-VF (i.e., 40th order using 2048 samples and 0.1 s of time-window), Fig. 4(a) presents an extended-time-window simulation of 0.2 s and using now only 512 samples. Although the time record of 0.1 s permits to capture the low-frequency dynamics, TD-VF starts showing a larger error, compared to NL-VF, for the 0.2 s time-window. An extreme case is presented in Fig. 4(b) where a rational model is obtained with a time record of 0.01 s and the simulation time-window is again 0.2 s with 512 samples. Fig. 4(b) shows that, although some low-frequency dynamics are missed, NL-VF still gives a smaller error than TD-VF. The results in Fig. 4 conclude that NL-VF is less sensitive to time-step and time-window length compared to TD-VF.

As an additional experiment, random noise with maximum magnitude of 10 is added to the voltage source $v_{dc}(t)$ and the capacitor voltage is calculated via NLT. These two variables are used again as input/output to both TD-VF and NL-VF to obtain two new rational models of order 40. Fig. 5 presents the absolute errors given by TD-VF and NL-VF for the capacitor voltage, $v_c(t)$. Fig. 5 shows that the latter is much less sensitive to noise in the TD input/output variables than TD-VF.

V. CASE STUDY 2: PHOTOVOLTAIC SYSTEM

A. System Description

The PV system of Fig. 6 is adopted from [11] to further illustrate the NL-VF approach. The system involves, besides

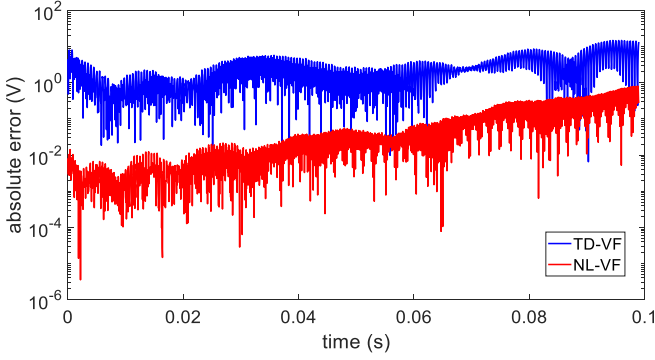


Fig. 5. Absolute errors by TD-VF and NL-VF for output $v_c(t)$ when the input is contaminated with random noise, using a time-window of 0.1 s and 2048 samples.

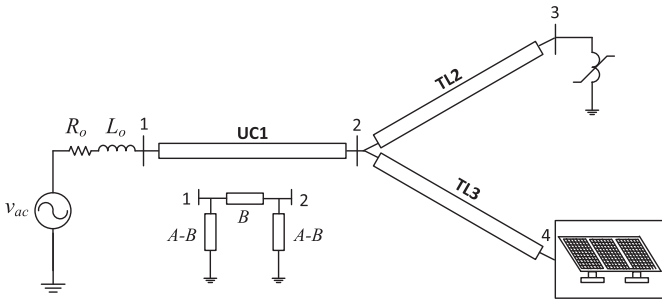


Fig. 6. PV system, adopted from [11].

a transmission network, a three-phase PV generator and a three-phase nonlinear reactor, connected at nodes 4 and 3, respectively. Within the PV generator, the PV modules are modeled as a Thévenin equivalent, i.e., a DC voltage source in series with a resistance [11]. The corresponding data can be found in [11]. The startup of the PV system is simulated in FD via the NLT algorithm with an observation time of 40 ms and considering 512 samples.

From the adopted NLT algorithm, the voltage at bus 4, $V_4(s)$, and the current across the filter inductor, $I_f(s)$, of the PV generator, are arbitrarily assumed as input and output, respectively, and fed into the NL-VF. Each of them is a FD column vector of dimensions 512 samples \times 3 phases = 1536 \times 1; note that only half of samples (positive frequencies only) plus DC component are used in the NL-VF approximation algorithm.

Fig. 7 presents the FD spectra, corresponding to phase a only, for both $V_4(s)$ and $I_f(s)$. It is observed in the spectra of Fig. 7 the presence of resonance peaks corresponding to the PV's inverter switching frequency of 2 kHz and its harmonics.

The initial set of poles in NL-VF is assumed as 150 complex conjugate poles that are linearly distributed. Ten pole iterations are utilized.

For verification purposes, the original output (I_f , phase a) provided by the NLT algorithm and the output given by the product between the approximated transfer matrix (given by NL-VF) and input FD vector, as in (4), are compared in Fig. 8(a). Both outputs are practically superimposed. Also, the absolute error is included in Fig. 8(a). The *rms* errors for the approximations are

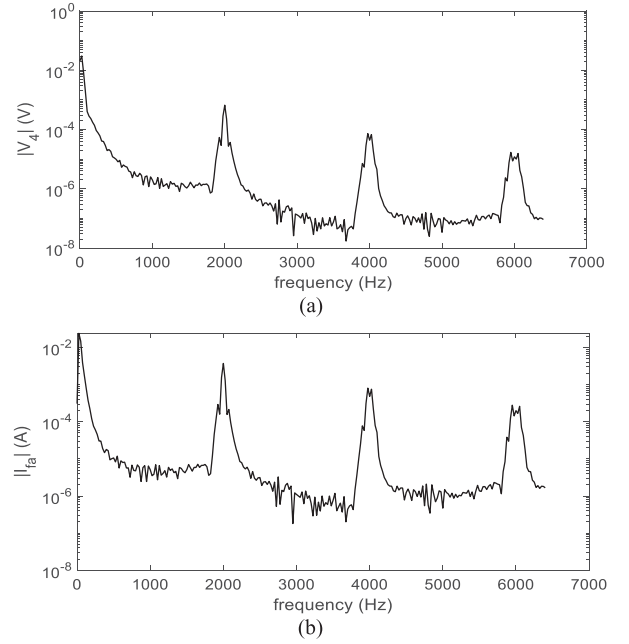


Fig. 7. FD spectra, corresponding to phase a , of (a) voltage at node 4, $V_4(s)$, and (b) current across the filter inductor, $I_f(s)$.

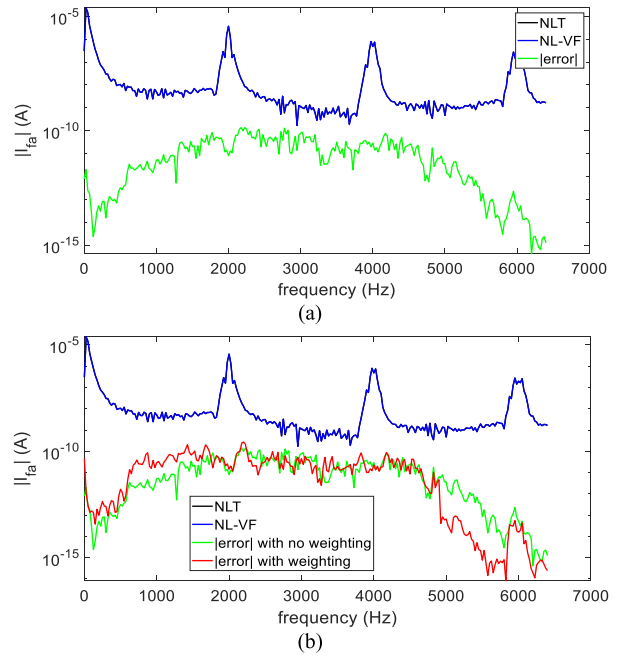


Fig. 8. Comparison of output $I_f(s)$ from NLT and NLT-VF for phase a (a) with no weighting and (b) with weighting for the last 60 samples.

of 3.45×10^{-11} , 2.93×10^{-11} , and 3.41×10^{-11} , for phases a , b , and c , respectively. The cpu-time by NL-VF is 11 s.

To highlight the control error feature of the NL-VF, which is not exhibited by TD-VF, Fig. 8(b) presents the results corresponding to Fig. 8(a) with a weight of 10 given to the last 60 samples of $\mathbf{Y}(s)$ [and last 60 rows of \mathbf{A} in (6)], in the range 4.9 kHz–6.4 kHz. Fig. 8(b) shows the effectiveness of weighting by the smaller absolute error obtained in the last 60 samples.

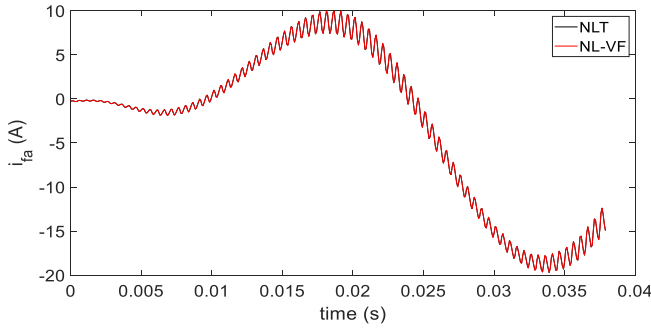


Fig. 9. Comparison of transient waveforms corresponding to $i_f(s)$, phase a , as given by NLT and NL-VF.

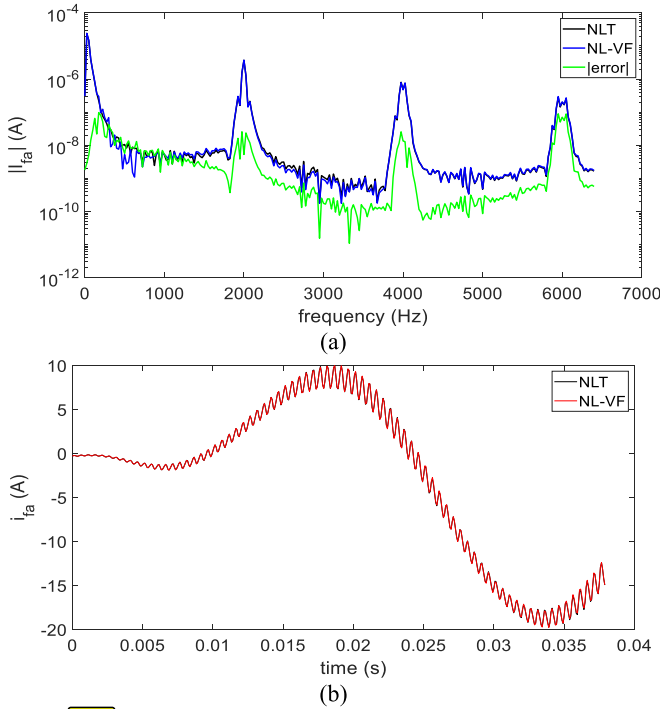


Fig. 10. Comparison of (a) output $I_f(s)$ as given by NLT and NL-VF for phase a using 5 pairs of complex poles and (b) corresponding transient waveforms.

Fig. 9 presents the transient waveforms corresponding to $i_f(t)$, phase a , as given by the NLT algorithm, and its approximated response via NL-VF. The rms error is of 1.72×10^{-7} .

Next, an extreme numerical experiment is performed. The NL-VF is now applied to this case study by using only 5 pairs of complex poles and ten iterations. Fig. 10 presents the spectra of the original output and its approximation via NL-VF and the corresponding transient waveforms. The rms errors for the FD approximation and TD waveforms are 1.54×10^{-8} and 5.28×10^{-5} , respectively. Fig. 10 shows that, despite the low order, a fair approximation is achieved and, furthermore, the dynamics of the system are reproduced with remarkable accuracy. The cpu-time is of 0.21 s, which represents around 2% of the cpu-time using 150 complex poles. This low-order rational model represents substantial computational savings when used to obtain the dynamic simulation of the system.

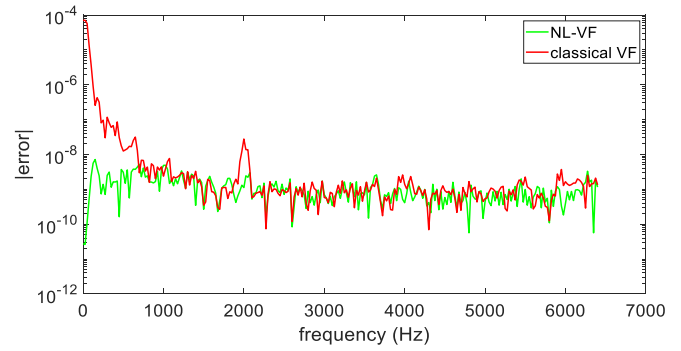


Fig. 11. Comparison of the approximation error for output $I_f(s)$ as given by NL-VF and classical VF for phase a using 150 complex poles.

Finally, a transfer matrix corresponding to the PV system of Fig. 6 is approximated by classical VF. The approximation errors for the output, phase a , as given by both NL-VF and classical VF are compared in Fig. 11. In both methods, 150 complex poles are used. In the overall, both approximations agree, noting that NL-VF provides a smaller approximation error in the low-frequency range.

VI. DISCUSSION

Although conceptually similar, the main difference between TD-VF and NL-VF is that the LS solutions of (3) and (4) are carried out in TD and FD, respectively. By using FD variables, NL-VF avoids numerical approximation of convolution integrals and very small time-step issues. Such FD variables are taken from the adopted NLT solution algorithm; nevertheless, other FD-based methods can be adapted to handle nonlinear components [16], [17], [18]. Alternatively, we can utilize any EMT-type software, such as EMTP-RV, PSCAD/EMTDC, or XTAP, to obtain the TD input/output variables for a given time-window [13], [14], [15]. These variables are then converted to FD via NLT and used within the NL-VF approach.

Similar to TD-VF, NL-VF is also applicable to any simulation time-window length despite a short time record. As shown in Fig. 4, the rational models by the two methods are prone to lose low-frequency dynamics and the accuracy deteriorates with simulation times being much longer than the time record. But the NL-VF was demonstrated to provide a smaller error in the transient response than TD-VF. Also, the excitation shape can have an influence in cases where some spectral components are inaccurately captured by the fitting. This is left as future research topic.

The primary objective of the paper is to compare NL-VF against TD-VF. Note that EMT-type models generally require a very small time-step to accurately reproduce high dynamics by electronic switches; moreover, it may require iterative methods when nonlinear components, represented as polynomial relations, are also included. In those cases, a rationally fitted model, such as NL-VF (or TD-VF), results advantageous. For example, the nonlinear circuit of Fig. 6 is accurately simulated by using 5 pairs of complex poles (Fig. 10), while the detailed EMT model

would involve a larger system of a combination of linear and nonlinear differential equations, including rational approximations for the lines/cable, switching devices, and nonlinear reactor.

In this paper, inverter-based systems, as the PV system in Section V, are under interest due to the presence of electronic switches. As further investigation, the combination of frequency-dependent network equivalents (FDNE) with equivalents of nonlinear systems, as given by NL-VF, will be considered.

Finally, a possible limitation of NLT-VF can be the dimensions of the LS solution system, as given by (6), when either $\mathbf{X}(s)$ or $\mathbf{Y}(s)$ or both have many resonance peaks in their frequency response, requiring a large number of samples. A preliminary solution utilized in this paper is to use positive frequencies only, translating in half cpu-time compared to using a complete FD vector with both positive and negative frequencies. This is also left as future research topic.

VII. CONCLUSION

An alternative FD-based fitting approach, named here as NL-VF, has been presented in this paper. A main application of NL-VF is to characterize, via rational functions, FD spectra of networks involving nonlinear loads and inverter-based networks. The input/output FD variables, used to obtain the fitted transfer matrix, are obtained from a FD-based simulation technique, i.e., the NLT, in a precise manner. It has been shown that, compared to the TD-VF approach, NL-VF does not present inaccuracies due to extended time-windows, it is less sensitive to noise, and exhibits error control via FD weighting.

APPENDIX A

The FD input/output relation of the boost circuit in Fig. 2 is described by

$$V_c = [(Y_c + Z_L^{-1} + S_b Z_o^{-1} S_b)^{-1} S_b Z_o^{-1}] V_{dc}. \quad (8a)$$

In (8a), S_b denotes a switching Toeplitz-type matrix with the frequency content of the corresponding switching function. Also in (8a), and based on the circuit of Fig. 2, we have:

$$Z_o = R_o + sL_o, \quad Z_L = R + sL, \quad Y_c = sC. \quad (8b)$$

APPENDIX B

The evaluation of (5) for M frequencies results in (6) where matrix \mathbf{A} is decomposed as $\mathbf{A} = [\mathbf{A}_1 \ \mathbf{A}_2 \ \mathbf{A}_3 \ \mathbf{A}_4 \ \mathbf{A}_5]$ with details given in (9), where subscripts a , b , and c denote the three-phases and subscript k stands for frequency sample. Due to space limitations, the submatrices in (9) present only one of their elements; the suspension points indicating frequency

evaluation downward and pole evaluation to the right.

$$\mathbf{A}_1 = \begin{bmatrix} \begin{bmatrix} \rho_r \\ \rho_i \end{bmatrix}_a & \dots \\ \begin{bmatrix} \rho_r \\ \rho_i \end{bmatrix}_b & \dots \\ \begin{bmatrix} \rho_r \\ \rho_i \end{bmatrix}_c & \dots \\ \vdots & \end{bmatrix}, \quad (9a)$$

where, for any phase and any real pole:

$$\begin{aligned} \rho_r &= \text{Re}\{Y(s_k)/(s_k - q_n)\} \\ \rho_i &= \text{Im}\{Y(s_k)/(s_k - q_n)\}, \end{aligned}$$

Also,

$$\mathbf{A}_2 = \begin{bmatrix} \begin{bmatrix} \alpha_r + \beta_r & -\alpha_i + \beta_i \end{bmatrix}_a & \dots \\ \begin{bmatrix} \alpha_r + \beta_r & -\alpha_i + \beta_i \end{bmatrix}_b & \dots \\ \begin{bmatrix} \alpha_r + \beta_r & -\alpha_i + \beta_i \end{bmatrix}_c & \dots \\ \vdots & \end{bmatrix}, \quad (9b)$$

where, for any phase and one pair of complex poles:

$$\begin{aligned} \alpha_r &= \text{Re}\{Y(s_k)/(s_k - q'_n)\} \\ \alpha_i &= \text{Im}\{Y(s_k)/(s_k - q'_n)\} \\ \beta_r &= \text{Re}\{Y(s_k)/(s_k - \text{conj}(q'_n))\} \\ \beta_i &= \text{Im}\{Y(s_k)/(s_k - \text{conj}(q'_n))\}, \end{aligned}$$

Also, equation (9c) shown at the top of next page, where, for any phase and any real pole:

$$\begin{aligned} \rho_r &= \text{Re}\{-X(s_k)/(s_k - q_n)\} \\ \rho_i &= \text{Im}\{-X(s_k)/(s_k - q_n)\}, \end{aligned}$$

Also,

$$\mathbf{A}_4 = \begin{bmatrix} \begin{bmatrix} N_a & N_b & N_c & 0 & 0 & 0 \end{bmatrix} & \dots \\ \begin{bmatrix} 0 & N_a & 0 & N_b & N_c & 0 \end{bmatrix} & \dots \\ \begin{bmatrix} 0 & 0 & N_a & 0 & N_b & N_c \end{bmatrix} & \dots \\ \vdots & \end{bmatrix}, \quad (9d)$$

where (similarly for N_b and N_c):

$$N_a = \begin{bmatrix} \alpha_r + \beta_r & -\alpha_i + \beta_i \\ \alpha_i + \beta_i & \alpha_r - \beta_r \end{bmatrix}_a, \quad (9e)$$

$$\mathbf{A}_3 = \begin{bmatrix} \begin{bmatrix} \rho_r \\ \rho_i \end{bmatrix}_a & \begin{bmatrix} \rho_r \\ \rho_i \end{bmatrix}_b & \begin{bmatrix} \rho_r \\ \rho_i \end{bmatrix}_c & 0 & 0 & 0 \\ 0 & \begin{bmatrix} \rho_r \\ \rho_i \end{bmatrix}_a & 0 & \begin{bmatrix} \rho_r \\ \rho_i \end{bmatrix}_b & \begin{bmatrix} \rho_r \\ \rho_i \end{bmatrix}_c & 0 \\ 0 & 0 & \begin{bmatrix} \rho_r \\ \rho_i \end{bmatrix}_a & 0 & \begin{bmatrix} \rho_r \\ \rho_i \end{bmatrix}_b & \begin{bmatrix} \rho_r \\ \rho_i \end{bmatrix}_c \\ \vdots & \vdots & \vdots & \vdots & \vdots & \vdots \end{bmatrix}, \quad (9c)$$

where, for any phase and one pair of complex poles:

$$\begin{aligned} \alpha_r &= \text{Re}\{-X(s_k)/(s_k - q'_n)\} \\ \alpha_i &= \text{Im}\{-X(s_k)/(s_k - q'_n)\} \\ \beta_r &= \text{Re}\{-X(s_k)/(s_k - \text{conj}(q'_n))\} \\ \beta_i &= \text{Im}\{-X(s_k)/(s_k - \text{conj}(q'_n))\}. \end{aligned}$$

\mathbf{A}_5 has the same structure as an instance of \mathbf{A}_1 with

$$\begin{aligned} \rho_r &= \text{Re}\{-X(s_k)\} \\ \rho_i &= \text{Im}\{-X(s_k)\}. \end{aligned}$$

The state space vector in (6) is:

$$\mathbf{x} = [\mathbf{x}_1 \quad \mathbf{x}_2 \quad \mathbf{x}_3 \quad \mathbf{x}_4 \quad \mathbf{x}_5], \quad (10)$$

where:

$$\begin{aligned} \mathbf{x}_1 &= [k_1 \quad \cdots \quad k_{n1}]^T \\ \mathbf{x}_2 &= [k'_{r1} \quad k'_{i1} \quad \cdots \quad k'_{rn2} \quad k'_{in2}]^T \\ \mathbf{x}_3 &= [[M_{11} \quad \cdots \quad M_{33}]_1 \quad \cdots \quad [M_{11} \quad \cdots \quad M_{33}]_{n1}]^T \\ \mathbf{x}_4 &= \begin{bmatrix} [M'_{11r} \quad M'_{11i} \quad \cdots \quad M'_{33r} \quad M'_{33i}]_1 & \cdots \\ [M'_{11r} \quad M'_{11i} \quad \cdots \quad M'_{33r} \quad M'_{33i}]_{n2} \end{bmatrix}^T \\ \mathbf{x}_5 &= [M_{11} \quad \cdots \quad M_{33}]^T \end{aligned}$$

The evaluation of (7) for M frequencies results in (6) with matrix \mathbf{A} decomposed now as $\mathbf{A} = [\mathbf{A}_1 \quad \mathbf{A}_2 \quad \mathbf{A}_3]$ where:

\mathbf{A}_1 has the same structure as an instance of \mathbf{A}_3 where, for any phase and any real pole:

$$\begin{aligned} \rho_r &= \text{Re}\{X(s_k)/(s_k - q_n)\} \\ \rho_i &= \text{Im}\{X(s_k)/(s_k - q_n)\}. \end{aligned}$$

\mathbf{A}_2 has the same structure as an instance of \mathbf{A}_4 where, for any phase and one pair of complex poles:

$$\begin{aligned} \alpha_r &= \text{Re}\{X(s_k)/(s_k - q'_n)\} \\ \alpha_i &= \text{Im}\{X(s_k)/(s_k - q'_n)\} \\ \beta_r &= \text{Re}\{X(s_k)/(s_k - \text{conj}(q'_n))\} \\ \beta_i &= \text{Im}\{X(s_k)/(s_k - \text{conj}(q'_n))\}. \end{aligned}$$

\mathbf{A}_3 has the same structure as an instance of \mathbf{A}_1 where, for any phase and any real pole:

$$\begin{aligned} \rho_r &= \text{Re}\{X(s_k)\} \\ \rho_i &= \text{Im}\{X(s_k)\}. \end{aligned}$$

The state space vector in (6) is now:

$$\mathbf{x} = [\mathbf{x}_1 \quad \mathbf{x}_2 \quad \mathbf{x}_3], \quad (11)$$

where:

$$\begin{aligned} \mathbf{x}_1 &= [[R_{11} \quad \cdots \quad R_{33}]_1 \quad \cdots \quad [R_{11} \quad \cdots \quad R_{33}]_{n1}]^T \\ \mathbf{x}_2 &= \begin{bmatrix} [R'_{11r} \quad R'_{11i} \quad \cdots \quad R'_{33r} \quad R'_{33i}]_1 & \cdots \\ [R'_{11r} \quad R'_{11i} \quad \cdots \quad R'_{33r} \quad R'_{33i}]_{n2} \end{bmatrix}^T \\ \mathbf{x}_3 &= [H_{\infty 11} \quad \cdots \quad H_{\infty 33}]^T \end{aligned}$$

The dimensions of \mathbf{A} in the evaluation of (5) are $(2 \times np \times M) \times (8 \times n_1 + 14 \times n_2)$, where M , np , n_1 , and n_2 denote number of frequency samples, phases, real poles, and complex poles, respectively. The dimensions of \mathbf{A} , \mathbf{b} , and \mathbf{x} in the evaluation of (7) are $(2 \times np \times M) \times (12 \times n_1 + 12 \times n_2)$.

REFERENCES

- [1] S. Grivet-Talocia and B. Gustavsen, *Passive Macromodeling: Theory and Applications*. New York, NY, USA: Wiley, 2016.
- [2] B. Gustavsen and A. Semlyen, "Rational approximation of frequency domain responses by vector fitting," *IEEE Trans. Power Del.*, vol. 14, no. 3, pp. 1052–1061, Jul. 1999.
- [3] S. Grivet-Talocia, "Package macromodeling via time-domain vector fitting," *IEEE Microw. Wireless Compon. Lett.*, vol. 13, no. 11, pp. 472–474, Nov. 2003.
- [4] Y. S. Mekonnen and J. E. Schutt-Aine, "Broadband macromodeling of sampled frequency data using z-domain vector-fitting method," *Proc. 2007 IEEE Workshop Signal Propag. Interconnects*, 2007, pp. 45–48, doi: [10.1109/SPI.2007.4512205](https://doi.org/10.1109/SPI.2007.4512205).
- [5] B. Gustavsen, "Improving the pole relocating properties of vector fitting," *IEEE Trans. Power Del.*, vol. 21, no. 3, pp. 1587–1592, Jul. 2006, doi: [10.1109/TPWRD.2005.860281](https://doi.org/10.1109/TPWRD.2005.860281).
- [6] D. Deschrijver, B. Haegeman, and T. Dhaene, "Orthonormal vector fitting: A robust macromodeling tool for rational approximation of frequency domain responses," *IEEE Trans. Adv. Packag.*, vol. 30, no. 2, pp. 216–225, May 2007, doi: [10.1109/TADVP.2006.879429](https://doi.org/10.1109/TADVP.2006.879429).

- [7] A. Beygi and A. Dounavis, "An instrumental variable vector-fitting approach for noisy frequency responses," *IEEE Trans. Microw. Theory Techn.*, vol. 60, no. 9, pp. 2702–2712, Sep. 2012, doi: [10.1109/TMTT.2012.2206399](https://doi.org/10.1109/TMTT.2012.2206399).
- [8] A. Ubolli and B. Gustavsen, "Comparison of methods for rational approximation of simulated time-domain responses: ARMA, ZD-VF, and TD-VF," *IEEE Trans. Power Del.*, vol. 26, no. 1, pp. 279–288, Jan. 2011.
- [9] N. M. Wereley, "Analysis and control of linear periodically time varying systems," Ph.D. dissertation, Massachusetts Inst. Technol., Cambridge, MA, USA, Feb. 1991.
- [10] P. W. Lehn and K. L. Lian, "Frequency coupling matrix of a voltage-source converter derived from piecewise linear differential equations," *IEEE Trans. Power Del.*, vol. 22, no. 3, pp. 1603–1612, Jul. 2007.
- [11] A. Ramirez, "Frequency domain modeling of photovoltaic systems for transient analysis," *IEEE Trans. Power Del.*, vol. 37, no. 5, pp. 3762–3770, Oct. 2022, doi: [10.1109/TPWRD.2021.3137273](https://doi.org/10.1109/TPWRD.2021.3137273).
- [12] A. Ramirez, "Frequency-domain computation of steady and dynamic states including nonlinear elements," *IEEE Trans. Power Del.*, vol. 24, no. 3, pp. 1609–1615, Jul. 2009.
- [13] J. Mahseredjian, S. Denetiere, L. Dube, B. Khodabakhchian, and L. Gerin-Lajoie, "On a new approach for the simulation of transients in power systems," *Electric Power Syst. Res.*, vol. 77, pp. 1514–1520, Sep. 2007.
- [14] *Manitoba HVDC Research Centre Inc.*, Winnipeg, MB, Canada: PSCAD, 1981.
- [15] eXpandable Transient Analysis Program (XTAP), CRIEPI-Japan, 2022. [Online]. Available: <https://www.xtap.org>
- [16] B. Gustavsen, "Validation of frequency-dependent transmission line models," *IEEE Trans. Power Del.*, vol. 20, no. 2, pp. 925–933, Apr. 2005.
- [17] N. Nagaoka and A. Ametani, "A development of a generalized frequency-domain transient program-FTP," *IEEE Trans. Power Del.*, vol. 3, no. 4, pp. 1996–2004, Oct. 1988.
- [18] A. Semlyen and M. R. Iravani, "Frequency domain modeling of external systems in an electro-magnetic transients program," *IEEE Trans. Power Syst.*, vol. 8, no. 2, pp. 527–533, May 1993.
- [19] P. Moreno and A. Ramirez, "Implementation of the numerical Laplace transform: A review task force on frequency domain methods for EMT studies, working group on modeling and analysis of system transients using digital simulation, general systems subcommittee, IEEE power engineering society," *IEEE Trans. Power Del.*, vol. 23, no. 4, pp. 2599–2609, Oct. 2008.

Abner Ramirez (Senior Member, IEEE) received the B.Sc. degree from the University of Guanajuato, Guanajuato, Mexico, in 1996, the M.A.Sc. degree from the University of Guadalajara, Guadalajara, Mexico, in 1998, and the Ph.D. degree from the Center for Research and Advanced Studies of Mexico (CINVESTAV), Guadalajara, Mexico, in 2001. From November 2001 to January 2005, he was a Postdoctoral Fellow with the Department of Electrical and Computer Engineering, University of Toronto, Toronto, ON, Canada. He is currently a Faculty Member with CINVESTAV. His research interests include electromagnetic transient analysis in power systems and power quality. He is a Member of the Mexican Association of Professionals and Entrepreneurs (APEM).

Bjørn Gustavsen (Fellow, IEEE) was born in Norway in 1965. He received the M.Sc. and Dr. Ing. in electrical engineering from the Norwegian Institute of Technology, Trondheim, Norway, in 1989 and 1993, respectively. Since 1994, he has been with SINTEF Energy Research, where he is currently a Chief Research Scientist. Since 2020, he has also been an Adjunct Professor with the Norwegian University of Science and Technology, Trondheim, Norway. His research interests include simulation of electromagnetic transients and modeling of frequency dependent effects. In 1996, he was a Visiting Researcher with the University of Toronto, Toronto, ON, Canada, and the summer of 1998 with the Manitoba HVDC Research Centre, Winnipeg, MB, Canada. from August 2001–August 2002, he was Marie Curie Fellow with the University of Stuttgart, Stuttgart, Germany.

Isaias Ramirez (Member, IEEE) received the B.A.Sc. and M.A.Sc. degrees from the Facultad de Ingenieria Mecanica Electronica y Electronica (FIMEE), Salamanca, Mexico, in 1990 and 1999, respectively, and the Ph.D. degree in electrical engineering from the University of Waterloo, ON, Canada, in 2009. He is currently a Researcher with INEEL, Cuernavaca, México. His research interests include nano materials, outdoor insulation, insulation coordination, electromagnetic transients in power systems, nonlinear system behavior of photovoltaic systems and its interconnection to the grid, and virtual education.